VISIR, A TASTE OF SCIENTIFIC POTENTIAL

VISIR, THE ESO-VLT INSTRUMENT MADE FOR OBSERVATIONS IN THE TWO MID-INFRARED ATMOSPHERIC WINDOWS (THE SO-CALLED N- AND Q-BANDS), IS NOW PRODUCING SCIENTIFIC RESULTS. SOME FIRST RESULTS ARE DISCUSSED FROM A PEDAGOGIC POINT OF VIEW, EMPHASISING THE VARIOUS MECHANISMS AT WORK THAT PRODUCE MID-INFRARED RADIATION (THERMAL DUST EMISSION, TRANSIENTLY HEATED DUST EMISSION, ION LINE EMISSION, PURE ROTATIONAL LINE EMISSION OF MOLECULAR HYDROGEN, SYNCHROTRON EMISSION). THE TWO KEY ADVANTAGES OF VISIR, I.E., ITS HIGH ANGULAR RESOLUTION AND ITS HIGH SPECTRAL RESOLUTION, ARE ILLUSTRATED RESPECTIVELY BY THE RESULTS FROM THE OBSERVATIONS OF THE BROWN DWARF BINARY SYSTEM ε INDI, AND BY KINEMATIC STUDIES OF THE GALAXY NGC 7582.

ERIC PANTIN[1,4], PIERRE-OLIVIER LAGAGE[1], ARNAUD CLARET[1], CORALIE DOUCET[1], ANDREAS KAUFER[4], HANS-ULRICH KÄUFL[4], JAN-WILLEM PEL[2,3], REYNIER F. PELETIER[2], RALF SIEBENMORGEN[4], ALAIN SMETTE[4,5], MICHAEL STERZIK[4]

[1]DSM/DAPNIA/SERVICE D'ASTROPHYSIQUE, CEA/SACLAY, SACLAY, FRANCE; [2]KAPTEYN INSTITUTE, GRONINGEN UNIVERSITY, GRONINGEN, THE NETHERLANDS; [3]ASTRON (NETHERLANDS FOUNDATION FOR RESEARCH IN ASTRONOMY), DWINGELOO, THE NETHERLANDS; [4]EUROPEAN SOUTHERN OBSERVATORY, [5]F.N.R.S. BELGIUM

VISIR, THE VLT MID-INFRARED Imager and Spectrometer, was installed at UT3 (Melipal) in early 2004 and was successfully commissioned between May and August 2004 (Lagage et al., 2004). After this, the time until its planned start of regular science operations in period 75 (April–September 2005) has been used to integrate the instrument into the Paranal operations and maintenance schemes and to carry out some first Guaranteed Time Observations (GTO) by the instrument consortium and Science Verification (SV) observations to demonstrate the scientific capabilities of the instrument. A complete list of GTO and SV programs can be found at *http://www.eso.org/observing/proposals/gto/visir* and *http://www.eso.org/science/vltsv/visirsv*. The data from the Commissioning and SV observations are available to the public and can be retrieved through the ESO science data archive (*http://archive.eso.org*).

Since June 2004, the sensitivities of VISIR were carefully monitored through a systematic program of observations of standard stars as often as possible. Figures 1 and 2 show a compilation of these measured sensitivities both in the imaging and the spectroscopic mode. As seen on these figures, the sensitivities are in reasonable agreement with the predicted ones. However, the last 6 months of monitoring have shown that the sensitivity of VISIR depends quite significantly on the conditions of the weather and the observations conditions (seeing, airmass, amount of Precipitable Water Vapour; the value of the latter can be found at *http://www.eso.org/genfac/pubs/astclim/forecast/meteo/ERASMUS/par_fore.txt*). Mid-infrared observations with VISIR will thus benefit greatly from the flexibility provided by service observing scheduling since the constraints of the observer will be much better matched to weather and observation conditions. One should also note that some spurious effects, such as detector striping, may degrade the sensitivity performance sporadically.

A sample of first scientific results from VISIR has been selected to give a first taste of the overwhelming scientific potential of this latest VLT instrument.

VARIOUS ORIGINS OF MID-INFRARED RADIATION

EMISSION OF LUKEWARM DUST GRAINS IN THERMAL EQUILIBRIUM

Dust grains (silicates, amorphous carbon, graphite ...) immersed in a radiation field reach thermal equilibrium at the temperature that corresponds to the balance between absorbed and re-radiated energy. Depending on the circumstances (orbit, central source luminosity, chemical composition) they can reach a temperature of around 100–500 K. Their re-emitted energy is mostly radiated at infrared wavelengths, such that:

$\lambda_{max} = 2898/T$ µm, T in K (Wien's law).

Hence, a warm dust grain at room temperature (i.e., around 300 K), radiates its maximum energy at around 10 µm. Mid-infrared wavelength (10 and 20 µm) windows are thus well adapted to probe dust grains in orbits around a star, typically in the planetary zone (1–50 AU). As a result, the search for footprints left by planets very close to the star in dusty discs is possible. Figure 3 illustrates this with images of the dust-disc of β-Pictoris observed without coronograph (in contrast to visible and near-infrared observations) allowing one to study structures in the innermost regions; from these observations, the mechanism of disc replenishment can be inferred (collisions of planetesimals producing small particles) (Pantin et al. 1997; Pantin et al. 2005, in preparation) and the structure of the disc gives precious indications about the presence of gravitational perturbers, such as massive planets.

Generally speaking, in the mid-IR one is approaching the Jeans limit. Thus, the contrast between the stellar photospheres and the circumstellar environment is more favorable as compared to the near-IR, where coronography is a must.

EMISSION OF VERY SMALL DUST PARTICLES AND PAH

Very small dust grains (e.g. silicates, graphite, with sizes smaller than 0.01 µm) as well as polycyclic aromatic hydrogenated grains (PAH or "big" molecules formed of benzene rings) can be heated quite far away from a source, provided that the source emits a sufficient number of visible or ultraviolet photons. These photons stochastically heat these small grains (or big molecules) temporarily to temperatures close to 1000 K. The grains then relax through vibrational modes of C-H and C-C bonds, at a few precise wavelengths mainly found in the mid-infrared range (3.3 µm, 6.2 µm, 7.7 µm, 8.6 µm, 11.3 µm ...).

The ISO infrared satellite discovered that some isolated Herbig AeBe (HAEBE) stars

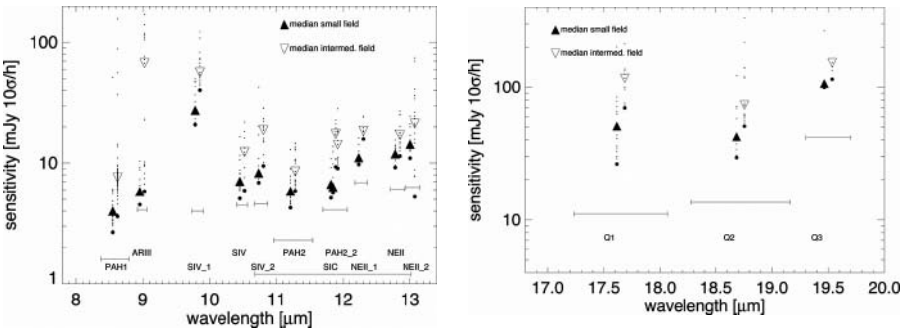

Figure1: Imager sensitivity monitored over 6 months, in *N*-band (left), and *Q*-band (right). The sensitivity is estimated for each standard star observation using the following method. One determines the radius at which the signal-to-noise is maximal. The star signal is integrated within this optimum radius and the corresponding error is computed. The sensitivity is finally deduced from the calibrated flux of the star deduced from Cohen et al. (1999) all sky network database of infrared calibrators. The horizontal bars represent the theoretical limits of VISIR sensitivity, the black dots show the "best ever" value of sensitivity reached. Note that the two pixel scales available ("small field" and "intermediate field") have differing sensitivities. Although not expected when modeling VISIR sensitivity, "small field" sensitivities are systematically better than "intermediate field" ones.

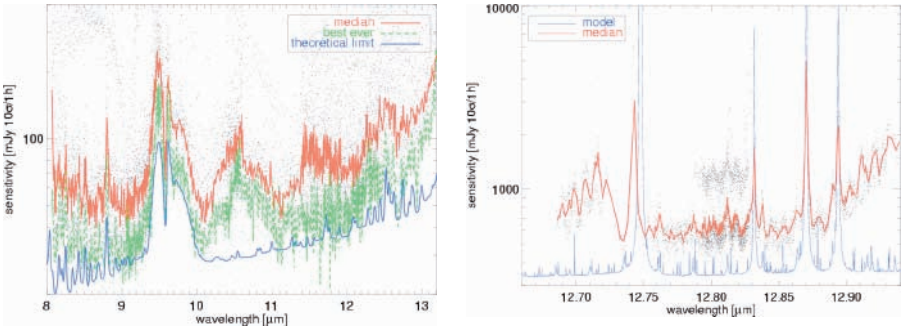

Figure 2: Spectrometer sensitivity monitored over a period of 6 months. The left panel shows the low-resolution mode in all four settings currently offered spanning the full *N*-band. The right panel displays the sensitivity measured in the long-slit [NeII] setting at 12.8 μm.

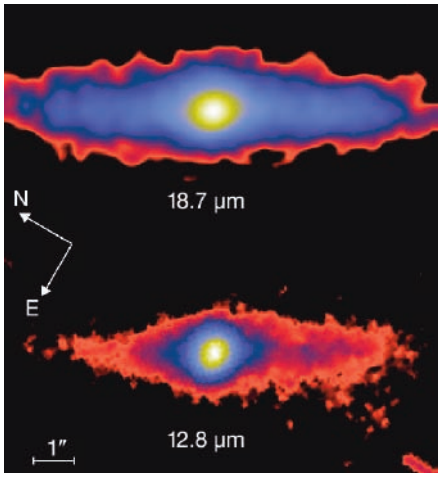

Figure 3: The dust disc of β-Pictoris seen by VISIR at 12.8 and 18.7 μm. The asymmetry (South-West side brighter than North-East side) is clearly seen. As illustrated here, the longer the observing wavelength, the colder the dust probed. However, the spatial resolution is also worse because of the diffraction limit. One key question that will be addressed with the above images is the following: is there an inner tilt in the β-Pictoris dust disc, as claimed from Keck observations (Wahhaj et al. 2003, Weinberger et al. 2003), or not, as claimed from recent Gemini observations (Telesco et al. 2005). Some more data processing (image deconvolution) is needed before having the VLT view!

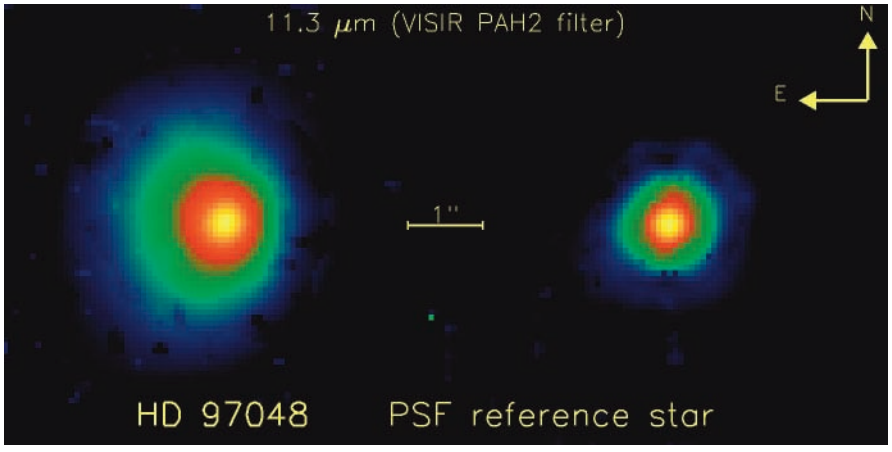

Figure 4: Image of the Herbig Ae star HD 97048. The extension seen in the "PAH" band filter centred on 11.3 μm is clearly visible. Such an extension cannot be explained just by thermal emission of dust grains at an equilibrium temperature and a population of small grains or PAH molecules transiently heated has to be invoked to explain the extension (Doucet et al. 2005). The spectroscopic observations (see Figure 5) indicate that a 11.3 μm feature attributed to PAH is indeed present. As expected the extension at 11.3 μm is larger than that observed recently at 3.3 μm with NACO (Habart et al.,2005, in preparation). A striking feature of the extension is its asymmetry. Sophisticated models including PAH, flaring disc geometry, viewing angle, inclination … are now needed to interpret these observations.

harbour dusty discs in which planetary formation is suspected to take place, and show the signature of such PAH (Waelkens et al. 1997, Waters et al. 1998).

One key programme of the VISIR guaranteed time observations is devoted to the study of a large sample of such HAEBE pre-main-sequence stars. We have observed one of these stars (HD 97048, Figures 4 and 5) using VISIR in imaging mode (PAH2 filter centred on 11.3 µm) and spectrometry mode (low-resolution 11.4 µm setting). The 11.3 µm image shows a quite large extension (2–3 arcsec) that was already suspected from previous observations (van Boekel et al. 2004). The spectrum confirms that PAH emission is indeed prominent in this disc, while the right panel of Figure 5 proves that the PAH emission is indeed spatially extended.

Line emission from ionized gas

Narrow atomic gas emission lines are also powerful probes of the astrophysical conditions. The most famous ones in the *N*-band are [NeII] at 12.8 µm, [ArIII] at 8.992 µm, and [SIV] at 10.485 µm. Narrow band (R = 50–80) filters corresponding to these lines are available in the VISIR imager and long-slit mode of the spectrometer. Concerning other lines (e.g. [HI] at 12.36 µm, forbidden lines such as [NII] at 12.79 µm, or [NaIV] at 9.04 µm), a cross-dispersed mode of the spectrometer will be offered in the future. In Figure 6, we demonstrate the possibility of studying the spatial emission of the [NeII] line in the central regions of the Seyfert 2 galaxy NGC 1068. Indeed, after subtraction the 2D continuum emission interpolated from images taken through reference filters around 12.8 µm, one obtains a map of the pure [NeII] emission (right panel of Figure 6). One can notice that the [NeII] emission is extended and follows the Narrow-Line-Regions, but, most interestingly, unveils the South-East, dust-extincted component of the ionising cone, as predicted by the unified AGN model (Galliano et al. 2005).

Emission lines from pure rotational modes of molecular gas

Although this mode has not been offered to the community yet, VISIR has the capability to obtain spectra at very high resolution (R ~ 15 000 to 30 000) of "cold" molecular Hydrogen H_2 at 12.28 and 17.03 µm. The transitions accessible to VISIR correspond to the lowest lying rotational states of the vibrational ground-state of Hydrogen. This potential is demonstrated in Figure 7 showing the emission line at 17.03 µm produced in the Orion bar (Allers et al. 2004). As shown in the same figure, the velocity structure of this cloud might be inferred from the precise central wavelength of the H_2 emission line. Additional checks are needed, however, before definitely attributing the observed wavelength changes to velocity.

This type of observation from the ground is not easy because of a strong atmospheric emission line very nearby at 17.027 µm; the high spectral resolution of VISIR makes VISIR a powerful instrument to detect the H_2 line.

Precise wavelength calibration is routinely achieved using the sky spectra recorded in the data. The observed atmospheric lines are compared with those predicted from an atmospheric model based on a HITRAN radiation transfer model. Using a cross-correlation method, an accurate wavelength calibration is derived on the fly (see Figure 8).

This observing mode offers great potential for example for the search for cold H_2 in protoplanetary discs.

Synchrotron emission from compact objects

Charged particles rotating in a strong magnetic field generate synchrotron emission. The observed spectrum is usually close to

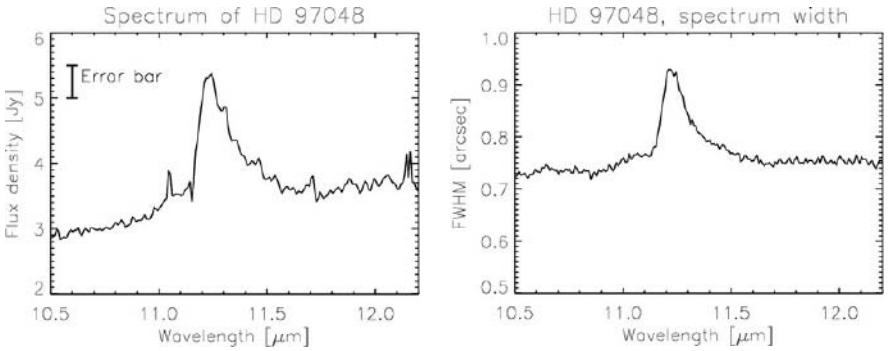

Figure 5: Left: Observed spectrum of HD 97048 around 11.4 µm in the long-slit low-resolution mode of VISIR. Right: The measured spatial full width at half maximum of the HD 97048 spectrum as a function of wavelength. The PAH emission at 11.3 µm is spatially more extended than the continuum and confirms the spatial extension of the image seen in Figure 4.

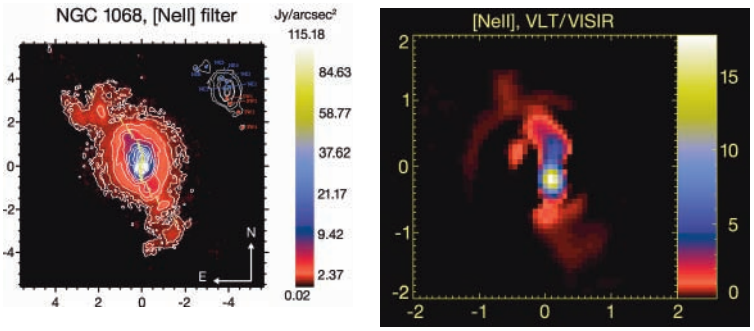

Figure 6: The Seyfert 2 galaxy NGC 1068. The left panel shows the image obtained through the NeII filter centered on 12.8 µm, and contains both the continuum and the gas emission. The yellow ticks overplotted mark the local position angle of the isophotes, showing the symmetrical twisting of the mid-infrared emission from the center to the outer parts of the AGN. Also shown is a sketch of the different knots identified in the image. The right panel shows the atomic emission line of [NeII] once the continuum component has been subtracted. Overplotted scales give the offset coordinates in arcseconds from the central engine position.

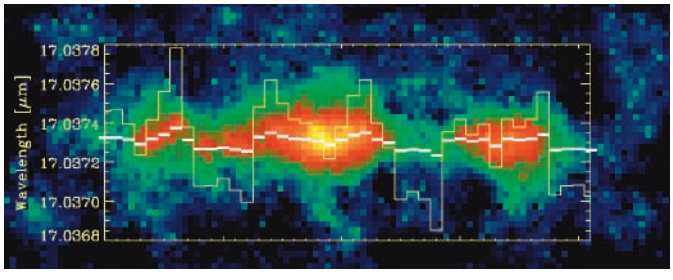

Figure 7: The Orion bar observed using VISIR in a long-slit, high-resolution setting at 17.03 µm. In the background is shown the 2D spectrum (dispersion direction is vertical, spatial direction is horizontal, North is to the left). The horizontal white bars overplotted pinpoint the local maxima of the emission line across the field. The yellow curve displays the corresponding central wavelengths as a function of the position in the field.

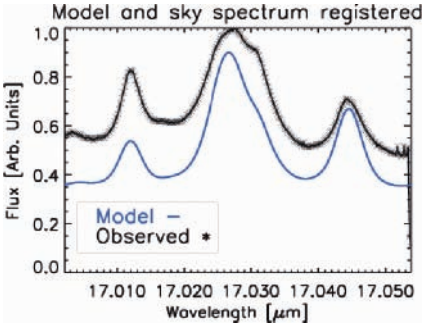

Figure 8: Wavelength calibration of the spectrometer using a cross-correlation method between the observed sky spectrum (black) and a model of atmospheric emission based on HITRAN computations (blue).

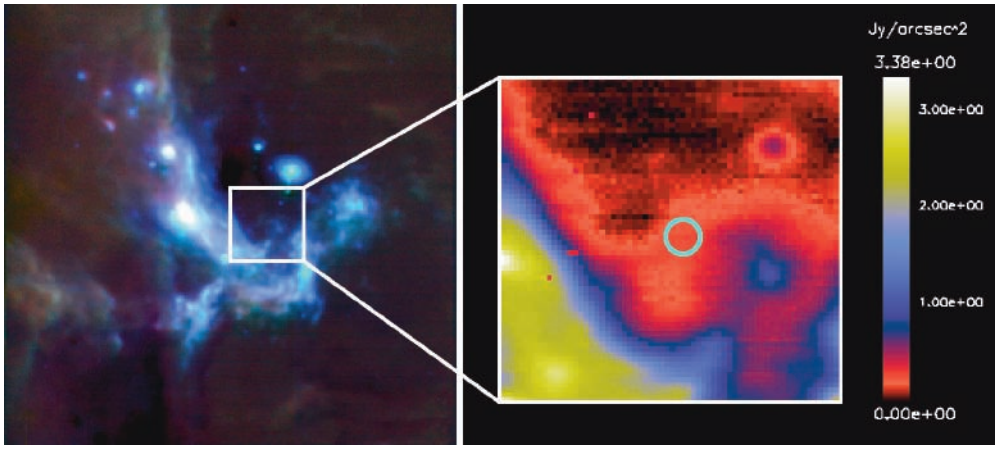

Figure 9: The Galactic Centre observed through the PAH1 (8.6 μm) filter. The goal is to detect the synchrotron emission from the black hole (position shown by the circle) and constrain its emission models.

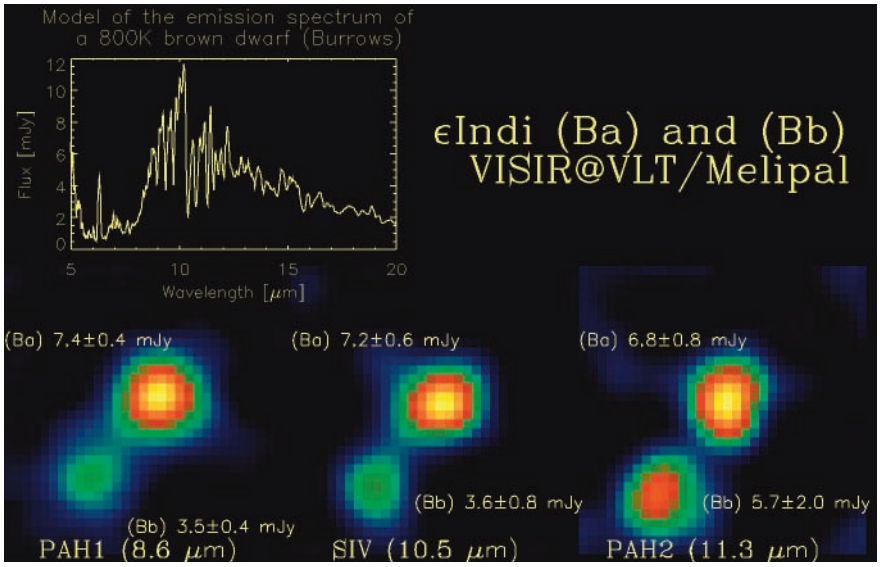

Figure 10: ε Indi, the closest binary brown dwarf, observed with VISIR in three filters (PAH1 (8.6 μm), SIV (10.4 μm), and PAH2 (11.3 μm)). We were able to spatially resolve both components, separated by ~ 0.73 arcsec, and determine accurate mid-infrared photometry for both components independently. In particular, our VISIR observations allowed us to probe the NH_3 features in both of the T1 (component Ba) and T6 (component Bb) cool brown dwarf. For the first time, we could disentangle the contributions of the two components, and find that the cold ε Indi Bb is in reasonable agreement with recent "cloud-free" atmosphere models. On the other hand, the warmer ε Indi Ba deviates significantly from any available atmosphere model calculations. It may or may not have clouds, and we might witness non-equilibrium chemical effects of NH_3 in ε Indi Bb. One should note that SPITZER could only measure a composite spectrum (Roellig et al. 2004).

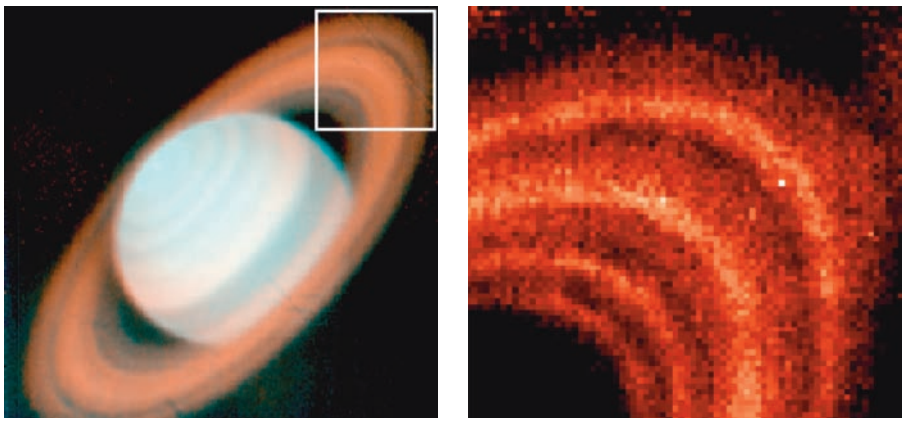

Figure 11: Left: Composite image of Saturn (blue = PAH2 filter at 11.3 μm, red = Q3 filter at 19.5 μm). The "shadow" region on the left side of the planet corresponds to ring particles with lower temperatures after cooling down in Saturn's shadow. Right: A close-up of Saturn's rings showing the D, C, B, and A rings (from left to right), Cassini's division between the B and A rings, and more interestingly, an increase of the particle temperature (hence increasing thermal emission) in the A ring just before entering the shadow of the planet.

a power-law function ($F_\nu \propto \nu^\alpha$ with α in the range 1–2) in the radio domain, peaking sometimes in the mid-infrared range as is the case for the black hole in Sgr A (Galactic Centre).

The very high extinction towards this object (A_V close to 30!) makes Sgr A impossible to detect in the visible range and quite difficult in the near-infrared range (Genzel et al. 2003).

We have monitored the Galactic Centre (see Figure 9) over four periods in order to try to detect the black hole mid-infrared emission. We could not catch it in its excited state (when it produces flares), but we could derive an upper limit of around 15 mJy for the flux in its quiescent state (Lagage et al. 2005, in preparation).

Key VISIR features: high angular resolution, high spectral resolution

High angular resolution: individual emission from a binary brown dwarf, Saturn's rings

One key advantage of VISIR over the SPITZER space observatory is the angular resolution. This is illustrated by two examples, the observations of binary brown dwarfs and Saturn's rings.

Cool stars and L and T brown dwarfs emit their energy maxima at wavelengths from the near-infrared up to 20 µm (Burrows et al., 2003), depending on their structure (dust settling, presence of "clouds", etc.) and effective temperature. We had the possibility to observe a binary brown dwarf during the science verification phase of VISIR in November 2004. As shown in Figure 10, we were able to detect the binary in the three filters with which we observed, and estimated the photometry of each of the components (SPITZER, although more suited to observe such faint objects, could only measure the spectrum of the two components and not distinguish each one separately). One can then put some constraints on the temperature, mass, and radius of each of the components (Sterzik et al. 2005, in preparation).

We observed Saturn's rings in May 2004, when the opening angle of the rings was maximal. VISIR images allow the study of the thermal emission from dust particles, and make it possible to spatially resolve the rings with a precision never reached before (see Figure 11) (Ferrari et al. 2005, in preparation). It is amazing that the resolution obtained with VISIR is equivalent to that obtained with the far-infrared focal plane FP1 of the CIRS (Composite InfraRed Spectrometer) instrument on board the Cassini spacecraft, at a distance of 20 Saturn radii during the CASSINI-HUYGENS Tour around Saturn between 2004 and 2008. CIRS will observe the rings at different wavelengths and under different viewing angles. This makes both instruments complementary. When observing such an extended object it is recommended to observe in imaging mode using jitter mode; i.e. some slight offset is applied between two nodding cycles, to avoid a significant number of bad pixels (~ 1%) affecting the final image.

High spectral resolution: Kinematics of warm gas in NGC 7582

The unique spectral resolution of VISIR in *N*-(R ~ 30 000) and *Q*-band (R ~ 15 000) allows us to resolve kinematically warm or ionized gas down to a limit of ~ 15 km/s. One example is shown in Figure 12. Here the dusty, composite starburst-Seyfert 2 galaxy NGC 7582 reveals its kinematic structure through the high spectral-resolution study of emission of ionized [NeII] gas at 12.8 µm, while the NeII filter image reveals the star-forming, circum-nuclear gas disc in the inner kiloparsec. The precision reached in velocity is around 18 km/s, and the spatial resolution of 0.4 arcsec corresponds to ~ 40 pc. From these data, one can infer an upper limit on the mass of central black hole (Wold et al. 2005, in preparation). This example shows the great potential of VISIR to study gas dynamics at high spatial resolution in the centres of galaxies.

More to come

VISIR will start science operation in visitor and service mode in P75. Only a selected number of instrument modes which could be properly characterised in the early phases of commissioning have been offered for the first proposal period. Additional modes and improved sensitivities in imaging and spectroscopy are planned to be offered for the coming observing periods. It is worth noting here that all offered instrument modes are fully supported by the newly developed VISIR (quick-look) pipeline which is available at the telescope and ESO Garching to process the data obtained in visitor and service mode. The latest information about the availability of the VISIR pipeline can be found at *http://www.eso.org/observing/dfo/quality/pipeline-status.html*. The latest information on the status of the instrument is available at *http://www.eso.org/instruments/visir/*.

Acknowledgements

We would like to thank the VISIR team at CEA, ASTRON and ESO for all their efforts to build and to bring into operation the VISIR instrument. We are further very grateful to C. Ferrari, E. Galliano and M. Wold for making some material available for this article prior to publication.

References

Burrows, A., Sudarsky, D. and Lunine, J. I. 2003, ApJ, 596, 587

Cohen, M. et al. 1999, AJ, 117, 1864

Galliano, E., Pantin, E., Alloin, S. and Lagage P.-O. 2005, MNRAS, submitted

Genzel, R. et al. 2003, Nature, 425, 934

Lagage, P.-O. et al. 2004, The Messenger, 117, 16

Pantin, E. et al. 1997, A&A, 327, 1123

Richter, M. J., Jaffe, D. T., Blake, G. A. and Lacy, J. H. 2002, ApJ, 572, L 161

Roellig, T. L. et al. 2004, ApJS, 154, 418

Telesco, C. et al. 2005, Nature, 433, 133

van Boekel, R. et al. 2004, A&A, 418, 177

Waelkens, C., Malfait, K., and Waters, L. B. F. M., 1997, Ap&SS, 255, 25

Waters, L. B. F. M. and Waelkens, C. 1998, ARA&A, 36, 233

Wahhaj, Z. et al. 2003, ApJ, 584, L 27

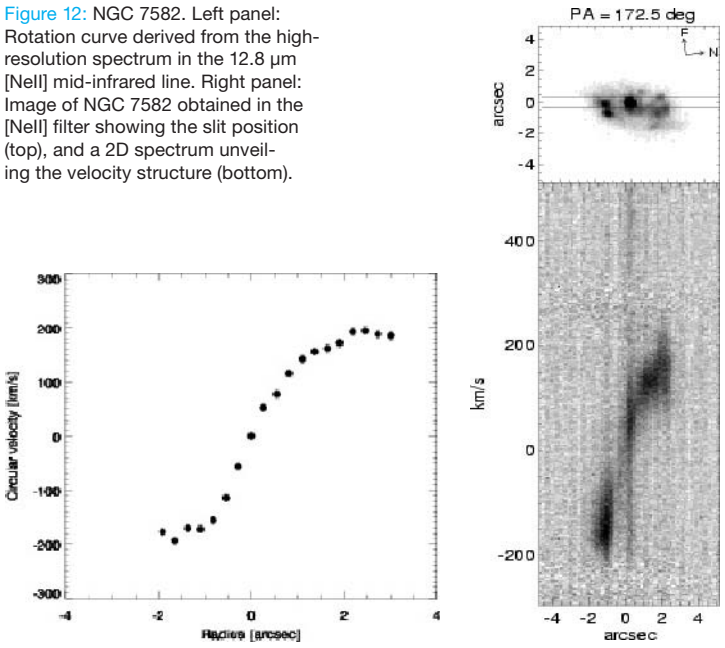

Figure 12: NGC 7582. Left panel: Rotation curve derived from the high-resolution spectrum in the 12.8 µm [NeII] mid-infrared line. Right panel: Image of NGC 7582 obtained in the [NeII] filter showing the slit position (top), and a 2D spectrum unveiling the velocity structure (bottom).